Impact of hydrothermal treatment of FEBEX and MX80 bentonites in water, HNO_3 and $Lu(NO_3)_3$ media: Implications for radioactive waste control

Francisco J. Osuna[1], Pablo Chain[2], Agustín Cota[3], Esperanza Pavón[1,4], María D. Alba[1*]

[1]Instituto Ciencia de los Materiales de Sevilla- Departamento de Química Inorgánica, CSIC-Universidad de Sevilla. Avda. Américo Vespucio, 49. 41092, Sevilla. Spain

[2]Consejería de Educación. Junta de Andalucía. 41092, Sevilla. Spain

[3] Laboratorio de Rayos-X. Centro de Investigación, Tecnología e Innovación de la Universidad de Sevilla (CITIUS), Universidad de Sevilla. Avda. Reina Mercedes, 4, 41012 Sevilla, Spain.

[4]Center for the Development of Nanoscience and Nanotechnology, CEDENNA, 9170124 Santiago, Chile

ABSTRACT

Engineered barriers of deep geological repositories (DGR) are commonly constructed with bentonite. FEBEX and MX80 bentonites have been selected by different countries as reference materials for the sealing of repositories; however, their chemical reactivity with high-level long-lived radioactive wastes (HLRW) under subcritical conditions had not been explored before. The hydrothermal stability in neutral and acid media and chemical reactivity in contact with an actinide analogous compound were both studied. The long-range and short-range structural changes were analyzed by X-ray diffraction, nuclear magnetic resonance and scanning electron microscopy. Both bentonites

*Corresponding author. Tel.: +34 954489546
E-mail address: alba@icmse.csic.es

have exhibited a good stability in neutral and acid media and have generated a new phase immobilizing the actinide analogous compound. The extent of the chemical reaction is higher in MX80 bentonite than in FEBEX bentonite.

Key Words—Bentonite, Engineered barrier, rare-earth, hydrothermal treatment, subcritical conditions, radioactive waste.

1. Introduction

The complexity of radioactive waste management is one of the most significant challenges faced by all countries involved in nuclear power generation. It is also a concern in many other countries using radioactive materials for medical, industrial, or research purposes. Radioactive wastes have to be disposed in ways that minimize their negative impact. In particular, the most hazardous and long-lived waste, such as spent nuclear fuel or reprocessing waste arising from the operation and dismantling of nuclear reactors, must be contained and isolated in order to ensure the long-term radiological protection of humans and the environment. Disposal of such waste in deep underground-geological repositories has become an effective and universally preferred option (Allègre, 1999; McCombie et al., 2000; Savage et al. 2010).

A deep geological repository (DGR), designed for the long-term management of high-level long-lived radioactive waste (HLRW), is a multi-barrier system consisting of engineered and backfill barriers surrounded by an additional geosphere barrier (Astudillo, 2001; Chapman, 2006; McCombie et al., 2000). Engineered barriers are commonly constructed with bentonite due to its low hydraulic conductivity and diffusivity and its high cation sorption capacity and buffering properties (Landais, 2006; Meunier et al., 1998; Pusch, 2006). In addition, bentonite retards the diffusion of radionuclides through sorption processes, and it is able to react with radioactive leachates (Bradbury and Baeyens, 2005; Coppin et al., 2002). The barrier, made of compacted bentonite (a highly swelling material), will get saturated with groundwater while it is subjected to high temperatures due to the radioactive decay of the wastes (Villar and Gómez-Espina 2008).

Under the conditions expected in HLRW repositories, alteration of a smectite (the main mineral component of bentonites) is expected to increase its hydraulic conductivity (permeability) and porosity and decrease its swelling pressure and cation exchange capacity (CEC) (Bildstein et al., 2006; Carlson et al., 2007; Gaudin et al., 2009; Savage et al., 2010). An alternative and effective immobilization mechanism that would overcome these drawbacks could involve the chemical retention of actinides by the bentonite. Lutetium disilicate ($Lu_2Si_2O_7$) is formed when a nitric acid solution of lutetium reacts with pure smectite under subcritical pressures and temperatures as it is expected to occur in Deep Geological Repositories (DGR), even after weathering of the smectite (Alba and Chain, 2005; Alba et al., 2009, Perdigón, 2002). Moreover, the persistence of $Lu_2Si_2O_7$ under hydrothermal conditions covering a wide range of pH and different salt solutions was demonstrated (Alba et al., 2009). Disilicate-phase synthesis was, therefore, proposed to be a possible long-term retention solution for trivalent actinide cations. In this sense, Chain et al. (2013) analyzed the structural properties of smectites that enhance their reactivity with Lu^{3+} ions and lead to formation of the disilicate phase. However, the international HLRW programs do not consider using purified smectite but raw bentonite as buffer in DGR for both logistic and economic reasons. In this sense, FEBEX and MX80 bentonites were selected by different countries as reference materials for the sealing of HLRW repositories (Tripathy et al., 2004; Villar and Gómez-Espina, 2008), but their capacity for immobilization of actinides by chemical reaction under subcritical condition need further investigations.

Both the chemical reaction and interaction of bentonites with groundwater can, however, modify their physical and chemical properties, thus decreasing their retention capacity (Pusch et al., 2007). The hydrothermal stability of clay minerals in water, basic

and acidic media is of great importance, particularly where radioactive waste confinement is concerned. Thus, a precise knowledge of the properties of clay minerals such as the long-term integrity of the bentonite when it is in contact with either acidic tailings pore water (in the case of slurry wall filter cake) or acidic stored mine water (in the case of acid mine drainage collection ponds), is, therefore, of crucial importance for the safety of radioactive waste disposal concepts.

In a previous study, Villa-Alfageme et al. (2014) studied the reactivity of bentonite with Eu^{3+}. They observed that $Eu3^{+}$ is immobilized in a higher amount than expected based on the CEC of the bentonite and concluded that an additional chemical mechanism may therefore participate to the immobilization. Since short-range study by NMR was not carried out, the extension and nature of the involved chemical reaction(s) were not evaluated. The main aim of this study is, therefore, to characterize the formation of $Lu_2Si_2O_7$ in the bentonites FEBEX and MX80 upon treatment with a Lu^{3+} solution under subcritical conditions, with the aim to study the structural changes occurred on the bentonite and quantify the disilicate phase formation, and the hydrothermal stability of the two bentonites in two media in which the reaction may take place, namely water and strong acid. Although Lu^{3+} is not the best rare earth element (REE) analogous compound for trivalent actinides most commonly found in high activity radioactive waste (Np, Am, and Cm) (Astudillo, 2001), it was chosen because the formation of rare-earth disilicates is common to all REE, with lutetium being the most reactive (Alba et al., 2009).

2. Materials and method

2.1.Materials

The two selected bentonites are the Spanish bentonite FEBEX and the American bentonite MX80. Those bentonites were provided by ENRESA Company (the Spanish Company in charge of radioactive wastes management) and CIEMAT, Spain.

Bentonite FEBEX is a Ca, Mg, Na-bentonite (predominantly Ca) extracted from the Cortijo de Archidona deposit (Serrata de Níjar, Almería, Spain). It contains more than 90 % w/w of montmorillonite and variable quantities of quartz, plagioclase, K-feldspar, calcite and cristobalite (Caballero et al., 1983, 2005; Lloret, 2004; Villar 2002). The structural formula of the montmorillonite component is $(Ca_{0.5}Na_{0.08}K_{0.11})(Si_{7.78}Al_{0.22})(Al_{2.78}Fe^{3+}_{0.33}Fe^{2+}_{0.02}Mg_{0.81})O_{20}(OH)_4$ and the bulk cation exchange capacity (CEC) of the bentonite is 158.2 meq/100 g (Galunin et al., 2011).

Bentonite MX80 is a Na-bentonite from Wyoming, USA. This bentonite consists mainly of montmorillonite (70–85 % w/w), but also contains quartz, feldspars and smaller quantities of cristobalite and calcite (Monts-H et al., 2005). The structural formula of the montmorillonite component is $(Ca_{0.2}Na_{0.36})(Si_{7.96}Al_{0.04})(Al_{3.1}Fe^{3+}_{0.18}Fe^{2+}_{0.16}Mg_{0.56})O_{20}(OH)_4$ and the bulk CEC of the bentonite is 102.1 meq/100 g (Galunin et al., 2011).

2.2. Hydrothermal treatments

300 mg of powdered bentonite and 50 mL of $7.3 \cdot 10^{-2}$ M $Lu(NO_3)_3 \cdot 3.6H_2O$ solution, distilled water or 0.01 M HNO_3 solution were transferred into a stainless steel T316SS hydrothermal reactor and heated to 300º C for 48 hours under autogenous pressure. Although geochemical waste degradation and waste/rock interaction processes in hydrothermal environments remain predictable up to temperatures of about 200 ºC, many

studies focused on simulating deep geological disposal conditions use temperatures up to 350 ºC to increase the reaction rates (Alba and Chaín, 2007; Allen et al., 1988; Mather et al., 1982; Savage and Chapman, 1982). The reactors were then cooled to room temperature and the solids separated by filtration, washed repeatedly with distilled water, and allowed to dry in air at 25 ºC.

2.3. Analytical methods

X-ray powder diffraction patterns (XRD) were obtained using a Bruker D8I instrument. This diffractometer is operated with a Ni-filtered Cu K_α radiation, at 40 kV and 40 mA. Diffractograms were obtained from 3 to 70° 2θ at a scan step of 0.05° 2θ and with a counting time of 3 s.

Scanning electron microscopy (SEM) observations of morphology and Energy Dispersive X-Ray Spectroscopy (EDX) analyses of chemical composition were performed at 20 kV with a JEOL JSM 5400 microscope , equipped with a LINK Pantafet probe (Oxford Link ISIS) allowing chemical analyses using a Si/Li detector with Be window.

^{29}Si and ^{27}Al solid state nuclear magnetic spectra (MAS NMR) were recorded with a magnetic field of 9.36 T using a Bruker DRX400 spectrometer equipped with a multinuclear probe. Powdered samples were packed in 4 mm zirconia rotors and spun at 12 kHz. ^{29}Si MAS NMR spectra were obtained at a frequency of 79.49 MHz using a π/6 pulse width of 2.7 μs and a delay time of 60 s. ^{27}Al MAS NMR spectra were recorded at 104.26 MHz with a π/20 pulse width of 1.1 μs and delay time of 3 s. Chemical shifts are reported in ppm with respect to tetramethylsilane for ^{29}Si and a 0.1 M solution of $AlCl_3$ for ^{27}Al. All

spectra were deconvoluted into single Gaussian-Lorentzian bands using a modified version of the Bruker Winfit program (Massiot et al., 2002). The fitted parameters were intensity, position, band-width, and Gaussian/Lorentzian ratio.

3. Results and discussion

3.1. Hydrothermal stability of bentonites

Structural changes in the long-range order of both bentonites after hydrothermal treatments with water and 0.01M HNO_3 were analyzed by XRD (Fig. 1). The XRD patterns of the raw bentonites (Fig. 1a and 1d) are consistent with the general (*hk*) and basal (*00l)* reflections of a smectite, with minor reflections corresponding to impurities of quartz (PDF 04-007-0522), cristobalite (PDF 04-008-7742), and feldspar (PDF 04-017-1349). The *060* reflections are observed at a distance between the reflection planes of 0.15 nm, typical of dioctahedral 2:1 phyllosilicates (Alba et al. 2001a). The *001* basal reflections corresponds to a d_{001} value of 1.47 nm for bentonite FEBEX and 1.23 nm for bentonite MX80 and are due to a water bilayer and monolayer, respectively, around the interlayer cations, mainly Ca^{2+} in bentonite FEBEX and Na^{+} in bentonite MX80 (Alba et al. 2001a).

The positions of the *hk* reflections of both bentonites do not change upon hydrothermal treatments (Fig. 1b, 1c, 1e and 1f), thus indicating that the basic structure of the silicates remained intact and that no other crystalline phase was formed. However, their widths and intensities changed after the hydrothermal treatments, especially in acidic media, indicating the occurrence of structural disorder, also evidenced by the more pronounced pattern background.

173 The position and intensity of the *00l* reflection of bentonite FEBEX does not
174 change after the hydrothermal treatments in water and acidic media. The hydrothermal
175 treatments did however cause the swelling of the bentonite MX80 layers up to a d_{001}
176 spacing of 1.42 nm in water medium and 1.52 nm in acidic medium. This swelling may be
177 due to the presence of cations with a higher hydration state. Similar results were observed
178 by Alba et al. (2001a, 2001b) after hydrothermal treatment where a leaching of divalent and
179 trivalent cations from the octahedral sheet with the replacement of Na^+ in the interlayer
180 space was observed.

181 The SEM micrographies (Fig. 2a-2c and Fig. 3a-3c) evidence the remaining
182 lamellar structure of the both bentonite after the hydrothermal treatments. The untreated
183 bentonites show EDX spectra (Fig. 2d and Fig. 3d) with the emission lines characteristic of
184 the elements found in their chemical composition. The hydrothermal treatment in water
185 (Fig. 2e and Fig. 3e) does not cause any change in their chemical composition, however,
186 the acid treatment (Fig. 2f and Fig. 3f) results in a decrease of the K, Ca and Na $K_{\alpha 1}$ lines
187 due to the replacement of the initial interlayer cations by those leached from the
188 framework. Finally, this treatment provokes a relative decrease of the intensity of the Si $K_{\alpha 1}$
189 line, in agreement with the observed decrease of the XRD reflections intensities of the
190 impurities.

191 Therefore, both bentonites show a good stability under hydrothermal treatment in
192 water and acidic media and the observed structural changes are more pronounced in the
193 acidic medium. Short-range structural effect of the acid treatment was therefore analyzed
194 by MAS NMR spectroscopy.

195 ^{29}Si MAS NMR spectra of the untreated bentonites (Fig. 4a and 4c) show two set of
196 signals, the main one is in the range of -100 to -80 ppm and is due to Q^3(mAl), typical

197 environment of smectite, and the second one is in the range of -100 to -115 ppm and is due
198 to Q^4(mAl) of the impurities (Engelhardt and Michel, 1987). The deconvolution parameters
199 of the ^{29}Si MAS NMR spectra (Table 1) show that the smectite Si environments are
200 different in the two bentonites. For FEBEX bentonite, the smectite contribution to the ^{29}Si
201 MAS NMR spectrum is reaching 94.5 %, with two signals at -93.33 ppm, Q^3(0Al), and -
202 88.05 ppm, Q^3(1Al), which is compatible with an octahedral configuration and with an
203 isomorphical substitution of Si by Al in the tetrahedral sheet (Alba et al., 2001b). The ^{29}Si
204 MAS NMR spectrum of MX80 shows a symmetric signal at -93.80 ppm due to Q^3(0Al),
205 reaching 79.7 % of the total Si of the spectrum. The shifts of the ^{29}Si resonance at lower
206 frequency is due to the lower total layer charge (Weiss et al., 1987) and the absence of
207 Q^3(1Al) environment is due to the lack of substitution of Si by Al in the tetrahedral sheet.
208 In both bentonites, the ^{29}Si MAS NMR spectra are compatible with their mineralogical
209 composition (Caballero et al., 1983; Lloret et al., 2004; Montes-H et al., 2005).

210 After the hydrothermal treatment in acidic medium, the Q^4 component is less
211 intense in the ^{29}Si MAS NMR spectra of MX80 bentonite (Fig. 4d, left) revealing a
212 diminution in the amount of impurities. The Q^3(0Al) component of MX80 is similar to that
213 of the untreated bentonite. In the FEBEX sample, the Q^3(1Al) contribution is lost,
214 indicating the leaching of tetrahedral Al.

215 The ^{27}Al MAS NMR spectra of the untreated bentonites (Fig. 4a and c, right) show
216 a main resonance centered at ca. 0 ppm, due to the octahedral Al environment and
217 compatible with the dioctahedral character of both bentonites (Engelhardt and Michel,
218 1987). Additionally, a small signal between 50 and 79 ppm is observed, due to Al in
219 tetrahedral coordination (Engelhardt and Michel, 1987). In both samples, a signal at 40-70
220 ppm is made of two signals; the main one at ca. 57 ppm is due to q^4 environment of

221 impurities, and, the very small one at ca. 65 ppm is due to q^3 environment in smectite phase
222 (Engelhardt and Michel, 1987). After the hydrothermal treatments in acidic medium, the
223 spectra (Fig. 4b and d, right) are quite similar to those of the untreated bentonite, the only
224 difference being that the q^4 environment of the impurities is absent, further indicating their
225 dissolution.
226
227 *3.2. Immobilization of actinides analogous compounds by bentonites under*
228 *hydrothermal conditions*
229
230 Structural changes in the long-range order of the bentonites after hydrothermal
231 treatment with Lu^{3+} solution were analyzed by XRD (Fig. 5). In general, *hk* reflections of
232 the montmorillonite and quartz and feldspar impurities mostly disappeared after the
233 treatment, thus indicating disruption of their basic structure (or dissolution). Only a small
234 *001* reflection is observed at a d_{001} of 1.49 nm which is caused by the partial swelling of the
235 layers, possibly due to the presence of trivalent cation Lu^{3+} in the interlayer space with a
236 higher hydration state than the original cations (Alba et al., 2001a). The intensity of the
237 basal reflections decreased, probably because of a lower-order stacking of the layers and
238 due to the partial transformation of the sample into kaolinite after the treatment.
239 The XRD patterns of the hydrothermally treated samples are dominated by the
240 kaolinite reflections (PDF 01-075-0938) and both bentonites present reflections
241 corresponding to $Lu_2Si_2O_7$ (PDF 00-035-0326), more intense for MX80 than for FEBEX.
242 Additionally, small reflections due to chrysotile (PDF 00-025-0645) are observed for
243 MX80.

Changes in short-range order produced by the hydrothermal treatment were studied by MAS NMR spectroscopic analysis of the active nuclei in the silicate (Fig. 6). The hydrothermal treatment of both bentonites resulted in ^{27}Al MAS NMR spectra (Fig. 6a and c, right) with a unique aluminum symmetric resonance at ca. 0 ppm, due to six-coordinated aluminum. The position at ca. 0 ppm and the low quadrupolar line shape of the band (symmetry band) are compatible with aluminum in the octahedral sheet of kaolinite (Engelhardt and Michel, 1987). The absence of both tetrahedral resonances is compatible with the disruption of the smectite framework (or its dissolution) and with the dissolution of the q^4 impurities of the initial samples.

After the treatment, a complete transformation of the ^{29}Si MAS NMR spectra is observed (Fig. 6b and d, left). On the one hand, the signals at ca. -110 ppm, Q^4(mAl) environment, disappear in good agreement with the absence of quartz, cristobalite and feldspar evidenced by XRD. On the other hand, the signal in the range of Q^3(mAl) environment shifted towards higher frequency, at ca. -91.7 ppm, and is the convolution of two Si environment, the Q^3(0Al) of kaolinite (Engelhardt and Michel, 1987) and Q^1 of $Lu_2Si_2O_7$ (Alba et al., 2001b). The similitude of both resonances does not allow a quantification of the Si contribution of kaolinite versus $Lu_2Si_2O_7$. Therefore, an analysis of the samples by SEM/EDX was carried out.

After the hydrothermal treatment in $Lu(NO_3)_3$ solution, the FEBEX sample shows a homogeneous morphology composed by lamellar particles (Fig. 7a), similar to those of the untreated bentonite (Fig. 2a). The chemical analyses by EDX (Fig. 7b-d) reveal that: (i) the Mg, Na, K and Ca $K_{\alpha 1}$ lines disappear as a consequence of the smectite framework disruption (or dissolution); (ii) the layers are mainly composed by Al and Si in a proportion typical of kaolinite; and; (iii) in some particles, the EDX spectra contain also Lu M_α, L_α and

268 L_β lines. No other particle with different morphology and/or higher content of Lu was
269 detected. Therefore, the chemical reaction between FEBEX bentonite and Lu^{3+} is at its
270 initial stage.

271 After the hydrothermal treatment in $Lu(NO_3)_3$ solution, the MX80 sample shows
272 two types of particles: (i) most particles have a lamellar morphology (Fig. 8b) with an EDX
273 spectra (Fig. 8d) characterized by Si and Al $K_{\alpha 1}$ lines in a proportion typical of kaolinite;
274 and, (ii) other particles are isolated compact spheres (Fig. 8b) with an EDX spectra
275 constituted by Si $K_{\alpha 1}$ lines and Lu M_α, L_α and L_β lines which corresponds to $Lu_2Si_2O_7$
276 phases.

277 Therefore, the chemical reaction between the actinides analogous component and
278 bentonite is more extensive in MX80 than in FEBEX. This observation is in agreement
279 with a previous study which concluded that a lower isomorphic substitution and Na^+ as
280 interlayer cations favor the reaction of formation of $Lu_2Si_2O_7$ (Alba et al., 2009).

281

282 **4. Conclusions**

283

284 The lamellar structure of FEBEX and MX80 bentonites remains intact after
285 hydrothermal treatment in water and only minor structural changes are observed after the
286 hydrothermal treatment in acidic medium. The only observed effect is the swelling of the
287 interlayer space which is associated to the replacement of original monovalent and/or
288 divalent cations by trivalent cations leached from the framework and the dissolution of the
289 impurities (quartz and feldspar). However, longer experiments may lead to additional
290 textural, chemical and structural changes.

Both bentonites are able to generate $Lu_2Si_2O_7$ phase under hydrothermal treatment at 300°C in $Lu(NO_3)_3$ solution simulating subcritical conditions. A large proportion of the montmorillonite component of the bentonites is transformed into kaolinite, which is likely to generate a substantial loss of CEC and may affect porosity and hydraulic conductivity of the clay materials due to volume changes. The formation of the insoluble immobilization phase $Lu_2Si_2O_7$ is however expected to minimize the impact of these possible changes by providing an additional immobilization mechanism to the clay barrier. Among the two bentonites, MX80 is the most efficient barrier material as a higher amount of insoluble $Lu_2Si_2O_7$ phase was generated compared to FEBEX in spite of its smaller smectite content. The lowest octahedral isomorphic substitution of the montmorillonite component of MX8O and the presence of Na^+ instead of Ca^{2+} in its interlayer space seem to favour the chemical reaction of bentonite with actinide analogous compound.

Acknowledgements

We would like to thank the Junta de Andalucía (Spain) and FEDER (Proyecto de Excelencia de la Junta de Andalucía, project P12-FQM-567) for providing financial support. We also thank to ENRESA (contract nº 0079000237) and CIEMAT for providing samples and by their support. Dr. Pavón also thanks her grant project, approved by the Andalucía Talent Hub Program launched by the Andalusian Knowledge Agency, co-funded by the European Union's Seventh Framework Program, Marie Skłodowska-Curie actions (COFUND – Grant Agreement nº 291780) and the Ministry of Economy, Innovation, Science and Employment of the Junta de Andalucía.

References

Alba, M.D., Becerro, A.I., Castro, M.A., Perdigón, A.C., 2001a. Hydrothermal reactivity of Lu-saturated smectites: Part I. A long-range order study. Am. Mineral. 86, 115-123.

Alba, M.D., Becerro, A.I., Castro, M.A., Perdigón, A.C., 2001b. Hydrothermal reactivity of Lu-saturated smectites: Part II. A short-range order study. Am. Mineral. 86, 124-131.

Alba, M.D., Chain, P., 2005. Interaction between Lutetium Cations and 2:1 Aluminosilicates under Hydrothermal Treatment. Clay Clay Miner. 53, 39-46.

Alba, M.D., Chain, P., 2007. Persistence of lutetium disilicate. App. Geoch. 22, 192-201.

Alba, M.D., Chain, P., Orta, M.M., 2009. Chemical reactivity of argillaceous material in engineered barrier Rare earth disilicate formation under subcritical conditions. App. Clay Sci. 43, 369-375.

Allègre, M., 1999. Geological repository: an unavoidable and ethically correct solution. In: Proceedings of the 24-th Annual International Symposium, London.Allen, C.C., Wood, M.I., 1988. Bentonite in Nuclear Waste Disposal: A Review of Research in Support of the Basalt Waste Isolation Project. App. Clay Sci. 3, 11-30.

Astudillo, J., 2001. El almacenamiento geológico profundo de los residuos radiactivos de alta actividad. Principios básicos y tecnología. *ENRESA*, Madrid.

Bildstein, O., Trotignon, L., Perronnet, M., Jullien, M., 2006. Modelling iron–clay interactions in deep geological disposal conditions. Phys. Chem. Earth 31, 618–625.

Bradbury, M., Baeyens, B., 2005. Modelling the sorption of Mn(II), Co(II), Ni(II), Cd(II), Eu(III), Am(III), Sn(IV), Th(IV), Np(V) and U(VI) on montmorillonites: linear free

energy relationships and estimates of surface binding constants for some selected heavy metals and actinides. Geochimica. Cosm. Acta 69, 875–892.

Caballero, E., Fernandes Porto, M.J., Linares, J., Reyes, E., 1983. Mineralogy, geochemistry and mineral genesis of bentonites from Serrata de Nijar (Almeria, Spain), Estudios Geológicos 39, 121–140.

Caballero, E., Jiménez de Cisneros, C., Huertas, F.J., Huertas, F., Pozzuoli, A., Linares, J., 2005. Bentonite from Cabo de Gata, Almería, Spain: a mineralogical and geochemical overview. Clay Min. 40, 463–480.

Carlson, L., Karnland, O., Oversby, V.M., Rance, A.P., Smart, N.R., Snellma, M., Vähänen, M., Werme, L.O., 2007. Experimental studies of the interactions between anaerobically corroding iron and bentonite. Phys. Chem. Earth 32, 334–345.

Chain, P., Cota, A., El Mrabet, S., Pavón, E., Pazos, M.C., Alba, M.D., 2013. Evaluation of rare earth on layered silicates under subcritical conditions: Effect of the framework and interlayer space composition. Chem. Geol. 347, 208-216.

Chapman, N., 2006. Geological disposal of radioactive waste — concept, status and trends. J. Iber. Geol. 32, 7–14.

Coppin, F., Berger, G., Bauer, A., Castet, S., Loubet, M., 2002. Sorption of lanthanides on smectite and kaolinite. Chem. Geol. 182, 57–68.

Engelhardt, G., Michel, D., 1987. High-resolution Solid-State NMR of Silicates and Zeolites. John Wiley & Sons, New York.

Galunin, E., Alba, M.D., Santos, M.J., Abrao, T., Vidal, M., 2011. Examination of competitive lanthanide sorption onto smectites and its significance in the magnagement of radiactive waste. J. Hazar. Mater. 186, 1930-1941.

360 Gaudin, A., Gaboreau, S., Tinseau, E., Bartier, D., Petit, S., Grauby, O., Foct, F.,
361 Beaufort, D., 2009. Mineralogical reactions in the Tournemire argillite after in-situ
362 interaction with steels. App. Clay Sci. 43, 196–207.
363 Landais, P., 2006. Advances in geochemical research for the underground disposal of high-
364 level, long-lived radioactive waste in a clay formation. J. Geochem. Expl. 88, 32–
365 36.
366 Lloret, A., Romero, E., Villar, M.V., 2004.FEBEX II Project. Final report on thermo-
367 hydro-mechanical laboratory tests. Publicación Técnica ENRESA 10/04. Madrid, pp
368 180.
369 Massiot, D., Fayon, F., Capron, M., King, I., Le Calvé, S., Alonso, B., Durand, J.O., Bujoli,
370 B., Gan, Z., Hoatson, G., 2002. Modelling one- and two-dimensional solid-state
371 NMR spectra. Mag. Reson. Chem. 40, 70-76.
372 Mather, J.D., Chapman, N.A., Black, J.H., Lintern, B.C., 1982. The geological disposal of
373 high-level radioactive waste-a review of the Institute of Geological Sciences
374 Research Programme. Nucl. Ener. 21, 167-173.
375 McCombie, C., Pentz, D.L., Kurzeme, M., Miller, I., 2000. Deep geological repositories: a
376 safe and secure solution to disposal of nuclear wastes. GeoEng2000 — An
377 International Conference on Geotechnical & Geological Engineering, Melbourne,
378 Australia. Technomic, Lancaster.
379 Meunier, A., Velde, B., Griffault, L., 1998. The reactivity of bentonites: a review. An
380 application to clay barrier stability for nuclear waste storage. Clay Clay Miner. 33,
381 187–196.

382 Montes-H, G., Marty, N., Fritz, B., Clement, A., Michau, N., 2005. Modelling of long-term
383 diffusion-reaction in a bentonite barrier for radiactive waste confinement. Appl.
384 Clay Sci. 30, 181-198.
385 Perdigón, A.C., 2002. Estudio del sistema saponita/$Lu(NO_3)_3/H_2O$ en condiciones
386 hidrotérmicas, Ph.D. thesis, University of Seville, Seville, Spain.
387 Pusch, R., 2006. Engineered barriers. In: Popov, V., Pusch, R. (Eds.), Disposal of
388 Hazardous Waste in Underground Mines. Wessex Institute of Technology, UK , pp.
389 35–40.
390 Pusch, R., Kasbohm, J., Pakovsky, J., Cechova, Z., 2007. Are all smectite clays suitable as
391 “buffers”. Phys. Chem. Earth 32, 116–122.
392 Savage, D., Chapman, N.A., 1982. Hydrothermal behaviour of simulated waste glass and
393 waste-rock interaction under repository conditions. Chem. Geol. 36, 59–86.
394 Savage, D., Watson, C., Benbow, S., Wilson, J., 2010. Modelling iron–bentonite
395 interaction. App. Clay Sci., 47, 91–98.
396 Tripathy, S., Sriharan, A., Schanz, T., 2004. Swelling pressure of compacted bentonites
397 from diffuse double layer theory. Can. Geot. J., 41, 437–450.
398 Villa-Alfageme, M., Hurtado, S., Castro, M.A., El Mrabet, S., Orta, M.M., Pazos, M.C.,
399 Alba, M.D., 2014. Quantification and comparison of the reaction properties of
400 FEBEX and MX-80 clays with saponite: Europium immobiliser under subcritical
401 conditions. Appl. Clay Sci., 101, 10-15.
402 Villar, M.V., 2002. Thermo-hydro-mechanical characterisation of a bentonite from Cabo de
403 Gata. A study applied to the use of bentonite as sealing material in high level
404 radioactive waste repositories. Publicación Técnica ENRESA 01/2002, pp 258.
405 Madrid.

406 Villar, M.V., Gómez-Espina, R., 2008. Effect of temperature on the water retention
407 capacity of FEBEX and MX-80 bentonites. Unsaturated Solids: Advances in Geo-
408 engineering**,** 257-262.
409 Weiss, C.A., Altaner, S.P., Kirpatrick, R.J., 1987. High-resolution ^{29}Si NMR spectroscopy
410 of 2:1 layer silicates: Correlation among chemical shift, structural distortions, and
411 chemical variations. Am. Miner. 72, 935-942.
412
413 .

414

415

416

Table 1. ^{29}Si chemical shift, linewidth (FWHM) and area under the curve of the different contribution obtained from the fitting of the ^{29}Si MAS NMR spectra of bentonite FEBEX and MX80: starting materials, and, after hydrothermal treatment at 300 ºC for 48 h in 0.01 M HNO_3 solution.

sample	δ (ppm)	FWWH (KHz)	%	Phase
Bentonite FEBEX				
raw	-88.05	0.819	18.4	Q^3(1Al)
	-93.33	0.325	76.3	Q^3(0Al)
	-110.34	0.661	5.3	Q^4(0Al)
treated in acid	-93.54	0.437	100	Q^3(0Al)
Bentonite MX80				
raw	-93.80	0.758	79.7	Q^3(0Al)
	-107.85	0.077	2.4	Q^4(0Al)
	-109.52	0.296	17.9	Q^4(0Al)
treated in acid	-93.41	0.536	89.0	Q^3(0Al)
	-107.87	0.118	11.0	Q^4(0Al)

FIGURE CAPTION

Fig. 1. XRD patterns of bentonite FEBEX (upper) and MX80 (down): (a, d) starting materials, and, after hydrothermal treatment at 300 ºC for 48 h in two different chemical media (b, e) water and (c, f) 0.01 M HNO_3 solution. q=quartz (PDF 04-007-0522), c=cristobalite (PDF 04-008-7742), and, f=feldspar (PDF 04-017-1349).

Fig. 2. SEM images and EDX spectra of bentonite FEBEX: (a,d) starting materials, and, after hydrothermal treatment at 300 ºC for 48 h in two different chemical media (b,e) water and (c,f) 0.01 M HNO_3 solution.

Fig. 3. SEM images and EDX spectra of bentonite MX80: (a,d) starting materials, and, after hydrothermal treatment at 300 ºC for 48 h in two different chemical media (b,e) water and (c,f) 0.01 M HNO_3 solution.

Fig. 4. ^{29}Si and ^{27}Al MAS NMR spectra of bentonite FEBEX (upper) and MX80 (down): (a, c) starting materials, and, (b, d) after hydrothermal treatment at 300 ºC for 48 h in 0.01 M HNO_3 solution.

Fig. 5. XRD patterns of bentonite FEBEX (upper) and MX80 (down): (a, c) starting materials, and, (b, d) after hydrothermal treatment at 300 ºC for 48 h in a $7.3 \cdot 10^{-2}$ M $Lu(NO_3)_3$ solution. q=quartz (PDF 04-007-0522), c=cristobalite (PDF 04-008-7742), f=feldspar (PDF 04-017-1349), cr=chrysotile (PDF 00-025-0645), k=kaolinite (PDF 01-075-0938), and, *=$Lu_2Si_2O_7$ (PDF 00-035-0326).

Fig. 6. ^{29}Si and ^{27}Al MAS NMR spectra of bentonite FEBEX (upper) and MX80 (down): (a, c) starting materials, and, (b, d) after hydrothermal treatment at 300 ºC for 48 h in a $7.3 \cdot 10^{-2}$ M $Lu(NO_3)_3$ solution.

Fig. 7. a) SEM images of bentonite FEBEX after hydrothermal treatment at 300 ºC for 48 h in a $7.3 \cdot 10^{-2}$ M $Lu(NO_3)_3$ solution. EDX spectra of bentonite FEBEX: (b) starting materials, and, (c,d) after hydrothermal treatment at 300 ºC for 48 h in a $7.3 \cdot 10^{-2}$ M $Lu(NO_3)_3$ solution.

443 **Fig. 8.** (a, b) SEM images of bentonite MX80 after hydrothermal treatment at 300 ºC for 48 h in a
444 $7.3 \cdot 10^{-2}$ M $Lu(NO_3)_3$ solution. EDX spectra of bentonite FEBEX: (c) starting materials, (d) lamellar
445 particles of Fig. 8.a., and, (e) the ball particles of Fig. 8.b.
446

447

448

449

450

Fig. 1

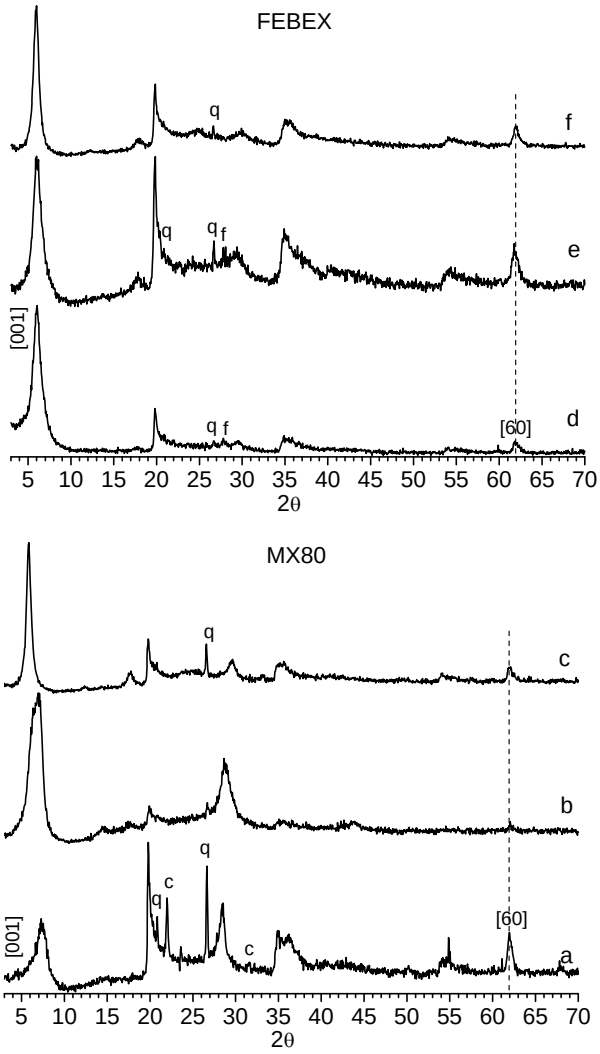

451

Fig. 2

452

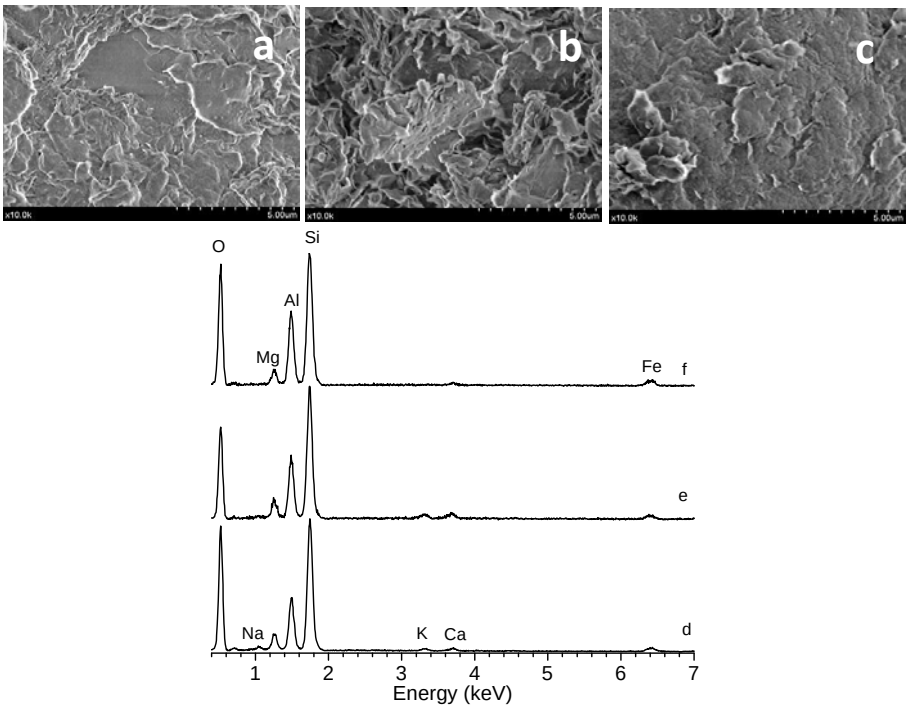

453 *Fig. 3*

454

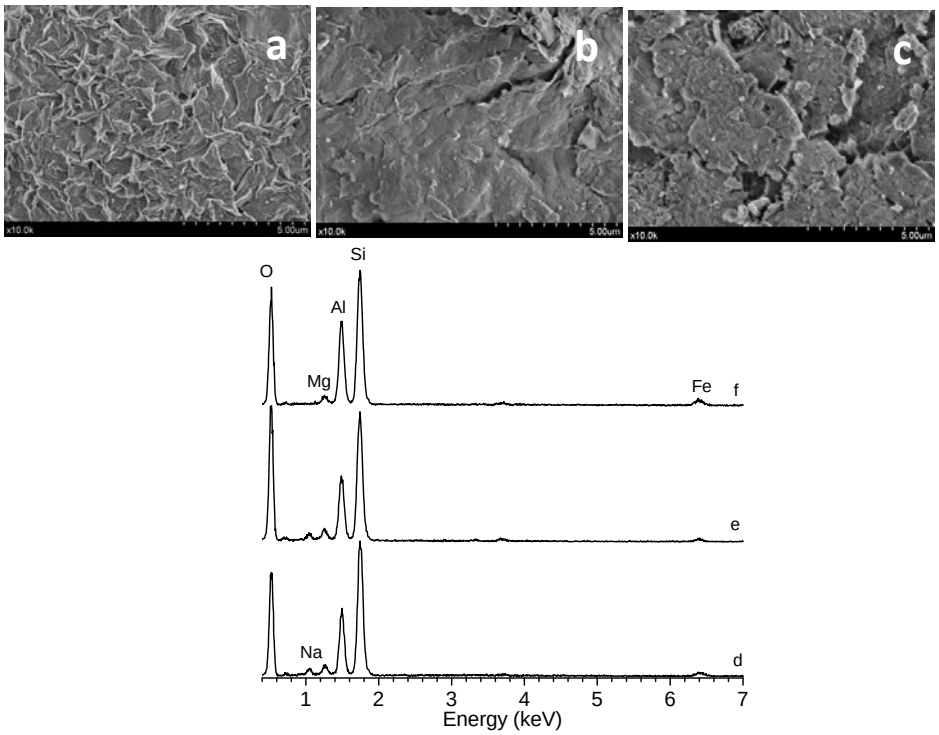

455

Fig. 4

456

457

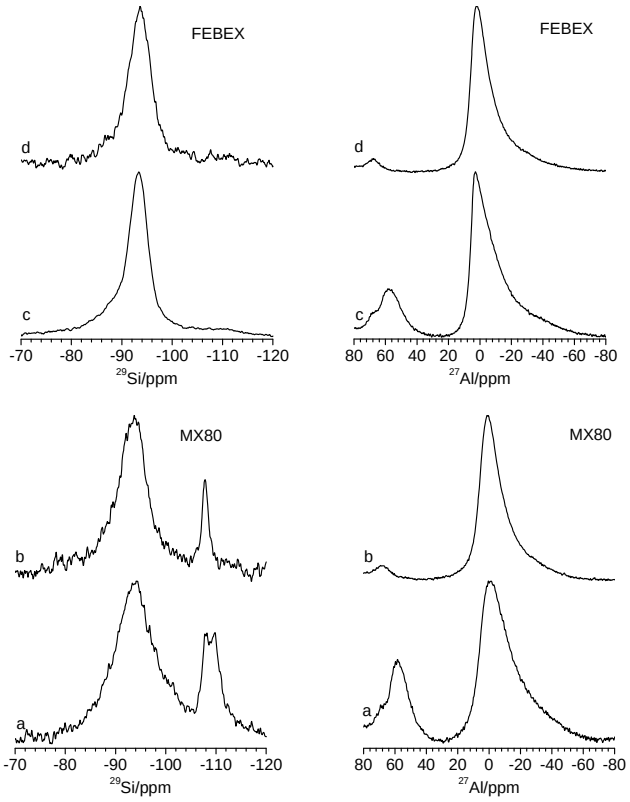

458

Fig. 5

459

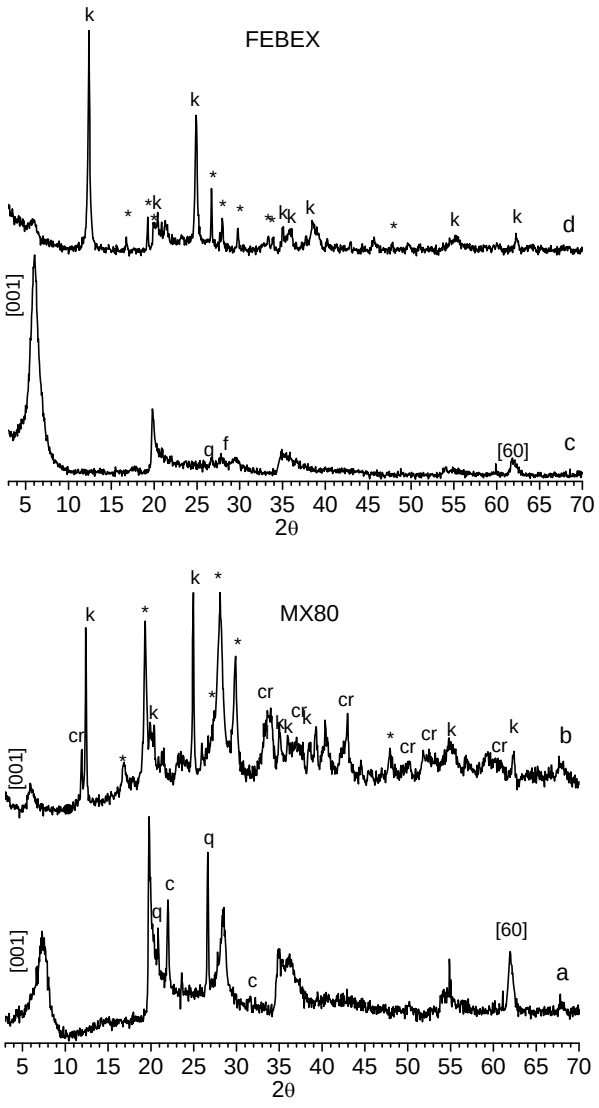

460

Fig. 6

461

462

463

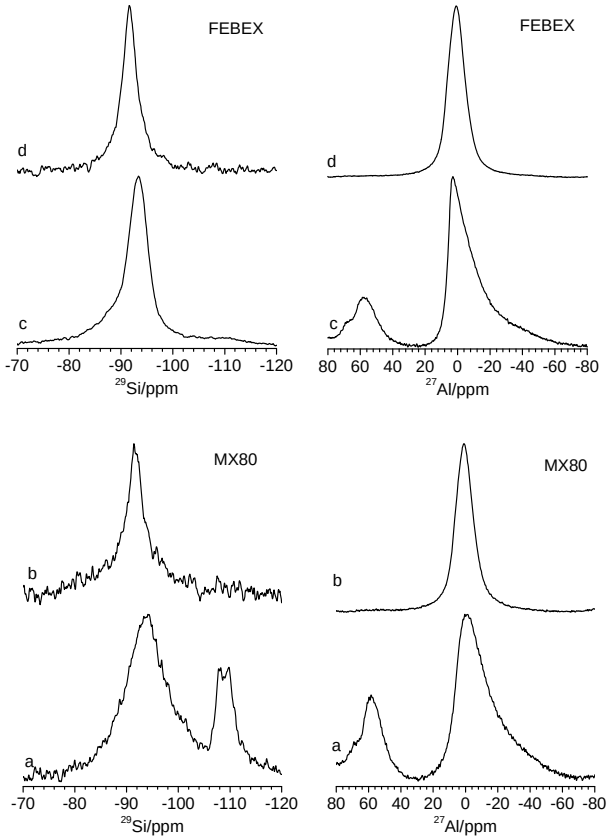

464

Fig. 7

465

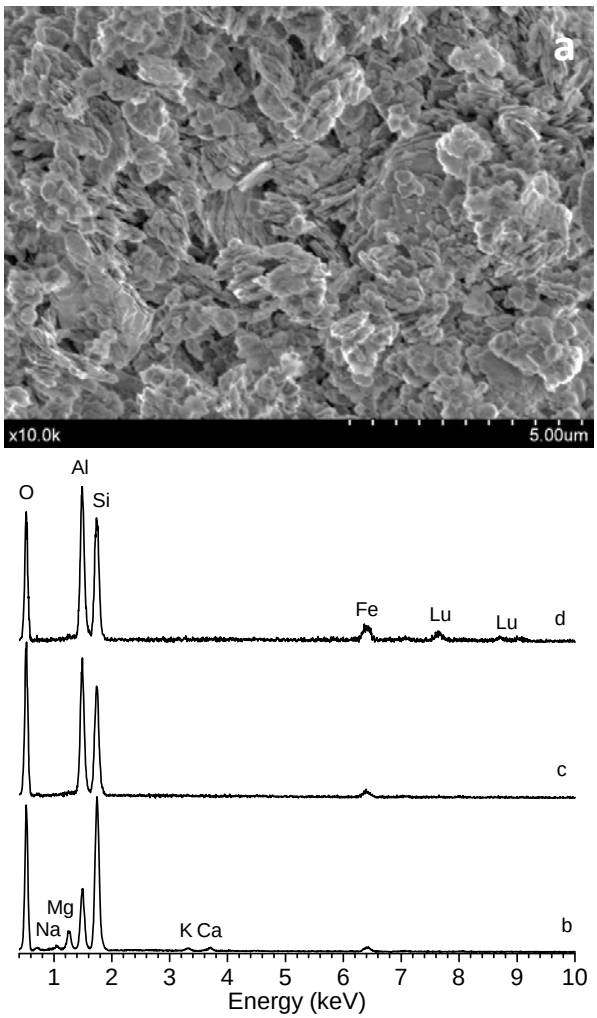
a
x10.0k
5.00um
O
Al
Si
Fe
Lu
Lu
d
c
Mg
Na
K Ca
b
1
2
3
4
5
6
7
8
9
10
Energy (keV)

466

Fig. 8

467

468